Geophys. J. Int. (2005) **161,** 891–906 doi: 10.1111/j.1365-246X.2005.02602.x

Magma intrusion and discharge process at the initial stage of the 2000 activity of Miyakejima, Central Japan, inferred from tilt and GPS data

Hideki Ueda,[1] Eisuke Fujita,[1] Motoo Ukawa,[1] Eiji Yamamoto,[1] Meilano Irwan[2] and Fumiaki Kimata[2]

[1]*National Research Institute for Earth Science and Disaster Prevention, Tennôdai 3-1, Tsukuba-shi, Ibaraki-ken,* 305-0006, *Japan. E-mails: ueda@bosai.go.jp (HU); fujita@bosai.go.jp (EF); ukawa@bosai.go.jp (MU); yamamoto@bosai.go.jp (EY)*

[2]*Research Center for Seismology, Volcanology and Disaster Mitigation, Graduate School of Environmental studies, Nagoya University, Furou-cho, Chikusa-ku, Nagoya-Shi,* 464-8602, *Japan. E-mails: irwan@seis.nagoya-u.ac.jp (MI); fumikimata@yahoo.co.jp (FK)*

Accepted 2005 February 8. Received 2004 November 26; in original form 2004 January 2

SUMMARY

The 2000 eruptive activity of Miyakejima island began with an earthquake swarm and crustal deformation that was clearly observed by continuous observations of ground tilt and GPS on Miyakejima. Based on the crustal deformation data, we estimated the magma migration process at the initial stage (18:30 LT on 2000 June 26—06:00 LT on 2000 June 27) of the activity. The activity in 2000 has been characterized by a collapse-caldera formation and no fissure eruption on the flank of the island, which is markedly different from the style of the recent eruptions in 1940, 1962 and 1983. We constructed a source model that approximately explains the crustal deformation data. The model consists of four dykes, of which three are intruding dykes and the other is a contracting dyke. We can infer the magma migration process at the initial stage from the model as follows. At 18:30 LT on June 26, the magma began to ascend from a dyke-shaped magma chamber and intrude at the southwestern flank of Miyakejima. In the intrusion, the total volume of intruded magma was $\sim 4 \times 10^6$ m^3. At around 21:00 LT, a relatively large volume of magma began to intrude as a dyke beneath the west coast of Miyakejima. The dyke then propagated laterally towards the northwest. The amount of magma intruded from 21:00 LT to 01:00 LT was $\sim 40 \times 10^6$ m^3. This large intrusion caused a discharge of magma from the magma chamber. The northwestward propagation of the dyke and the contraction of the chamber continued thereafter. The discharge of magma from the chamber beneath Miyakejima probably starved the first intrusion that had been ascending towards the southwestern flank of the island, resulting in the collapse-caldera formation after the initial stage. The style of the 2000 eruptive activity relative to recent activity has primarily been changed by the subsurface discharge of magma towards the northwest.

Key words: crustal deformation, dyke, GPS, magma chamber, Miyakejima volcano, tiltmeter.

1 INTRODUCTION

Observation of crustal deformation in volcanic areas provides useful information on subsurface magma movements and changes in magma systems. During the course of the 2000 Miyakejima eruptive activity, we successfully observed crustal deformation using networks of borehole tiltmeters and GPS. The data have been analysed to reveal the magma rising process mainly from the ground tilt data (Fujita *et al.* 2002a) and magma discharge process, mainly from GPS data (Nishimura *et al.* 2001). This study is aimed at modelling the magma migration process during the first day of the activity by combining ground tilt and GPS data.

Miyakejima island, located 170 km to the south of Tokyo, Japan (see Fig. 1 for its location), is an active stratovolcano of basaltic magma. An eruption had been expected around 2003, because the past three eruptions occurred in 1940, 1962 and 1983, at roughly 20-yr intervals (Miyazaki 1984). The typical style of the former three eruptions was a fissure eruption of basaltic lava on the flank of the volcano. Anticipating a future eruption, observational instruments had been deployed on the island by several institutes. The National Research Institute for Earth Science and Disaster Prevention (NIED) constructed five observation sites with borehole tiltmeters, seismometers and GPS receivers. The Geographical Survey Institute (GSI) of Japan, Tokyo University and the Japan Coast Guard deployed GPS stations.

The 2000 Miyakejima eruptive activity began at 18:30 LT (Japan Standard Time, UT+09:00) on 2000 June 26, accompanied by an earthquake swarm (Sakai *et al.* 2001) and rapid crustal deformation

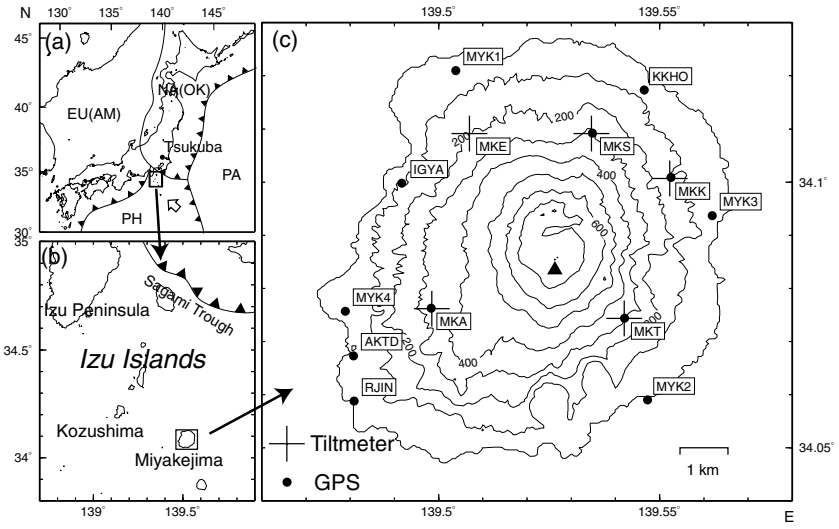

Figure 1. Guide map. (a) The tectonic environment around Izu island. EU, Eurasian Plate; AM, Amurian Plate; NA, North American Plate; OK, Okhotsk Plate; PA, Pacific Plate; PH, Philippine Sea Plate. The lines show plate boundaries. The open arrow indicates the direction of the plate motion of PH relative to EU (Seno *et al.* 1993). (b) Location of Miyakejima in Izu island. (c) Locations of tiltmeter stations (crosses) and GPS stations (circles) in Miyakejima. The triangle represents the summit of Miyakejima (814 m).

(Ukawa *et al.* 2000; Irwan *et al.* 2003). This activity has continued for more than 4 yr, with varying eruptive styles. From the observed geophysical data, ejecta and visible activity, the activity can be divided into four stages (Ukawa *et al.* 2000; Nakada *et al.* 2001). The first stage is the period from 18:30 LT on June 26 to the early morning of June 27, during which the magma rising process dominated. The second stage is the subsequent interval up to July 8, just before the first summit eruption. During this stage, magma that accumulated beneath Miyakejima moved to the northwest outside of the island. Small amounts of lava erupted west of Miyakejima in the early morning of June 27 (Shirao *et al.* 2000).

The third stage is defined as collapse-caldera formation at the summit area, probably as a result of the successive discharge of magmas from Miyakejima (Geshi *et al.* 2002). This stage began with the first summit eruption of July 8 and continued until late August, including several summit eruptions. The caldera formed for the first time in 2500 yr (Tsukui *et al.* 2001), characterizing the 2000 Miyakejima eruption. This stage is also characterized by the tilt steps indicating cyclic abrupt expansions of a magma chamber (Kumagai *et al.* 2001; Fujita *et al.* 2002b). The fourth stage is a volcanic gas emission period that began in late August. In the activity of 2000, unlike the recent eruptions, a fissure eruption did not occur.

The collapse-caldera formation, the tilt steps and the large volume of gas emissions in the long term clearly suggest a magma system with a large magma chamber in the upper crust beneath the island. The magma rising process in the initial stage is likely to be closely related to the magma system and the crustal deformation data undoubtedly contain key information that enables the understanding of the magma system. Up to now, the ground tilt data and the GPS data have been analysed separately mainly because of their different temporal resolution. Recently, Irwan *et al.* (2003) obtained crustal deformation data at 30-s intervals by applying kinematic GPS analysis.

In this study, we attempt to elucidate the subsurface magma migration process from 18:30 LT on June 26 to 06:00 LT on June 27. The reason for choosing this time interval is that the principal magma movements of this period were limited mostly to within Miyakejima, that is, in and around the observational network. In our analysis, we combine the ground tilt data and the GPS data to estimate model parameters for the magma system. The tilt data have high accuracy, but the number of stations is small and the estimated intrusion process is limited up to 01:00 LT on June 27 (Fujita *et al.* 2002a). The GPS data derive from a relatively larger number of stations and have better station coverage, but the accuracy of the vertical component is insufficient. No analysis combining both data sets had yet been carried out, but combining them would clearly provide the best model fitting crustal deformation induced by the subsurface magma movements. We applied a genetic inversion technique to solve the non-linear problem.

2 CRUSTAL DEFORMATION DATA

2.1 Tilt data

Tilt changes associated with the activity of 2000 were observed by a tiltmeter network established by NIED. The network consists of five borehole-type tiltmeters 100 m deep (see Fig. 1 for their locations), which are the force-balanced pendulum type (Sato *et al.* 1980). The data are continuously telemetered to NIED by telephone lines with a sampling rate of 1 Hz.

Fig. 2 shows the 1-min resampled tilt data of the stations in the period from 12:00 LT on June 26 to 12:00 LT on June 27. At 18:30 LT, tilt changes began with the earthquake swarm and the tilt change of MKT was initially the largest among the five stations. 2 hr later, a major tilt change towards the south began at MKA. The tilt change continued until 01:00 LT and amounted to 160 μrad. The tilt direction of MKA varied to the northeast at 01:00 LT, after which the tilt changes of all stations continued gently.

2.2 GPS data

The kinematic GPS data we used are 30-s-interval positional data analysed by Irwan *et al.* (2003), which were obtained from the dense GPS network in Miyakejima. The network consists of 12 stations (see Fig. 1 for their locations): the GSI set up MYK1, MYK2, MYK3

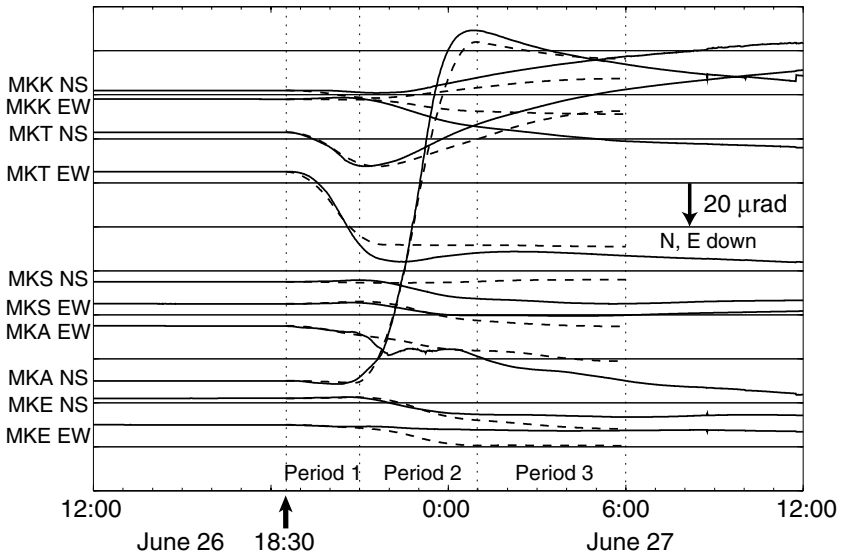

Figure 2. The tiltmeter records in the period from 12:00 LT on 2000 June 26 to 12:00 LT on 2000 June 27. Broken curves represent the theoretical tilt changes calculated from the dyke model. Vertical lines are the bounds of the periods.

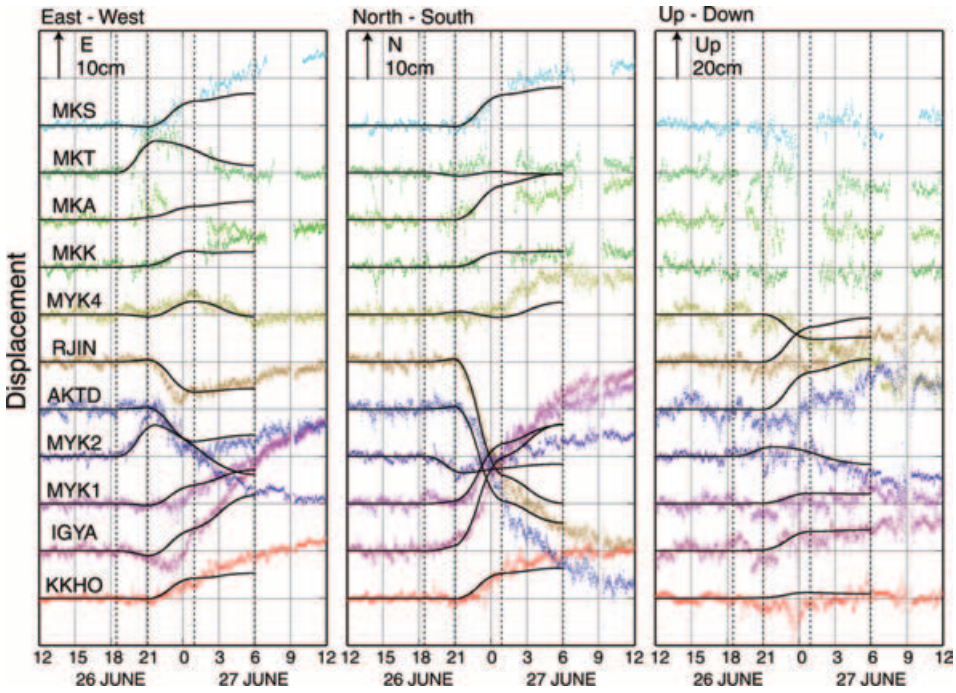

Figure 3. Time-series of 30-s coordinates of GPS sites in the period from 12:00 LT on 2000 June 26 to 12:00 LT on 2000 June 27. Curves represent the theoretical displacements calculated from the dyke model. Vertical lines are the bounds of the periods.

and MYK4; Tokyo University set up IGYA, KKHO and RJIN; the Japan Coast Guard installed AKTD; and NIED set up MKS, MKK, MKA and MKT. MYK3 is the reference station for the processing of kinematic GPS. The four NIED stations are single-frequency receivers and the others are dual-frequency receivers. The vertical components of the single-frequency receivers are not used in this study because of their large uncertainties.

The time-series of positions are shown in Fig. 3. Although the original data obtained by Irwan *et al.* (2003) are movements relative to MYK3, which are also moved by crustal deformation caused by volcanic activity, we corrected the data to be referenced to a station in Tsukuba (see Fig. 1a for its location). The station is distant enough from Miyakejima to obtain absolute movements resulting from volcanic activity. For this correction, we used 2-hr-interval GPS coordinates of MYK3 (Kariya *et al.* 2000), which is referenced to Tsukuba. Fig. 4 shows the time-series of movements of MYK3. The time-series were interpolated by polynomial functions in Fig. 4, after which we corrected the original data using these functions.

2.3 Temporal variation of crustal deformation

The tilt change and GPS data show that crustal deformation began at around 18:30 LT on June 26. The data also show the large crustal deformation between 21:00 LT on June 26 and 01:00 LT on June

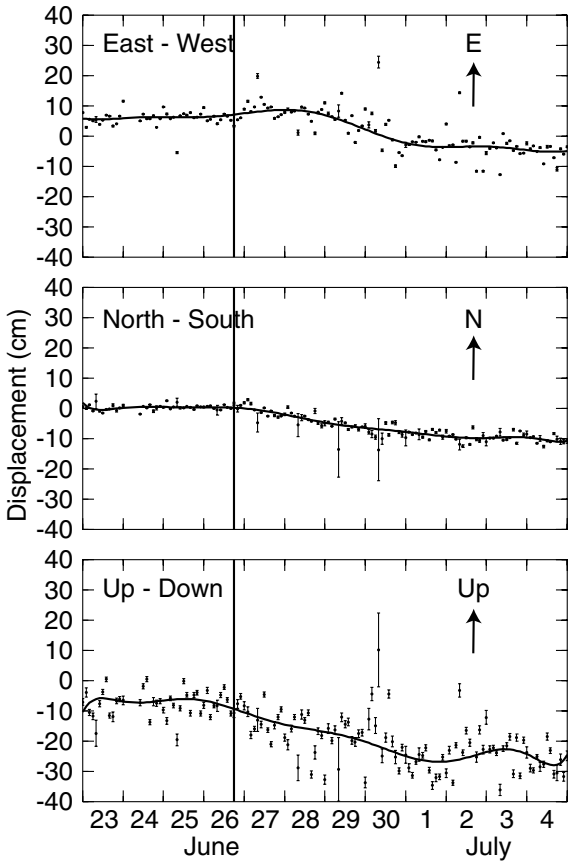

Figure 4. Time-series of 2-hr coordinates of MYK3 (Kariya *et al.* 2000), which is referenced to Tsukuba (see Fig. 1a for its location). Curves are the tenth degree polynomials fitted to the data. Vertical lines indicate 18:30 LT on June 26.

27. After this large deformation, the deformation rate gradually decreased. From these features, we divided the initial stage into three periods: period 1 (18:30 LT—21:00 LT on June 26), period 2 (21:00 LT on June 26—01:00 LT on June 27) and period 3 (01:00 LT—06:00 LT on June 27). The tilt vectors and the displacement vectors corresponding to the periods are plotted in Figs 5 , 6 and 7, respectively. The plotted displacements are differences between the mean positions in four periods: 12:00 LT—18:30 LT, 20:45 LT—21:15 LT, 00:45 LT—01:15 LT and 05:45 LT—06:15 LT. Because the four single-frequency receivers of NIED have blank periods in the time-series, we used means for the period from 02:00 LT to 02:30 LT rather than the period from 00:45 LT to 01:15 LT for these receivers.

Tilt-down vectors and displacement vectors in period 1 are shown in Fig. 5. In period 1, tilt changes in the southern part of the island predominate, especially at MKT, the tilt vector of which indicates tilting in the northeast direction. In the northern part of the island, by contrast, tilt changes were small, implying that the magma was intruding only into the southern part of the island. In this period, relatively large eastward horizontal displacements are seen at two stations in the southeastern part of the island.

Fig. 6 shows crustal deformation in period 2. The tilt change at MKA was very prominent. The tilt changes at the northern three stations also become clear in this period, suggesting that the crustal deformation was related to deeper magma movement than that in period 1. Extensional deformation in the northeast–southwest direction is dominant in the western part, strongly suggesting the intrusion

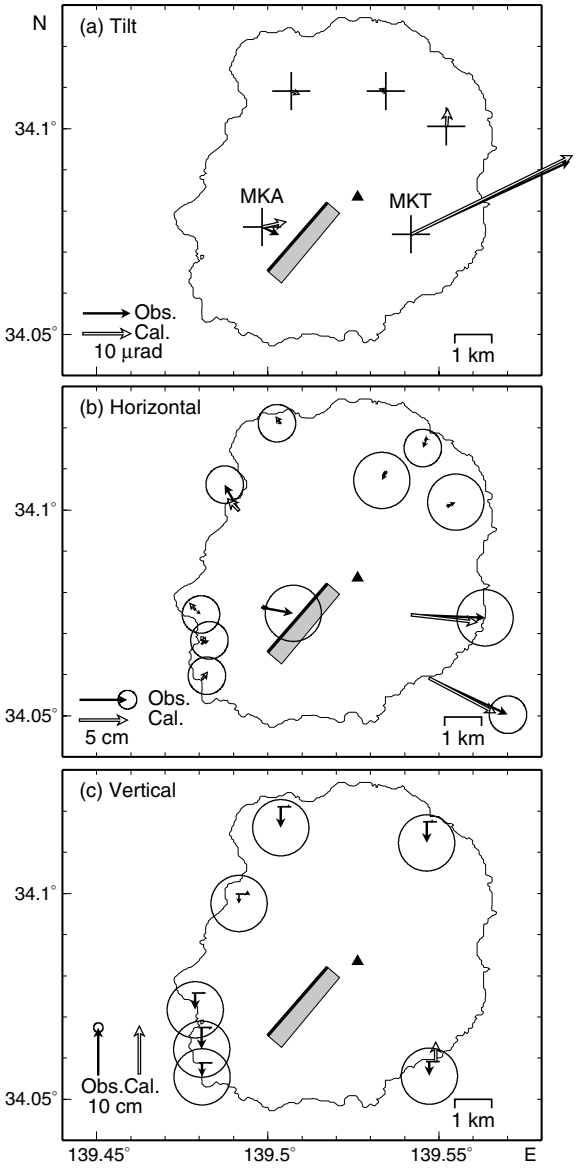

Figure 5. Observed crustal deformation of period 1 (18:30 LT–21:00 LT on June 26): (a) tilt-down vectors, (b) horizontal displacement and (c) vertical displacement vectors. Circles are standard errors of displacements. Blank arrows are the theoretical deformation calculated from the best-fitting dyke model, whose projection on the ground surface and the upper boundary are shown by rectangles and thick lines, respectively. The triangle represents the summit of Miyakejima.

of a dyke beneath the western part. In the southeastern part of the island, the horizontal displacements turn to the west.

Crustal deformation in period 3 is shown in Fig. 7. The tilt direction of MKA turns to the northeast. The displacements are basically similar to that of period 2, but with the minor difference of increased eastward components at the northwestern and southwestern stations.

3 MODELLING

3.1 Method

In modelling the sources of the crustal deformation at the initial stage, we assume that the dyke intrusion and propagation process

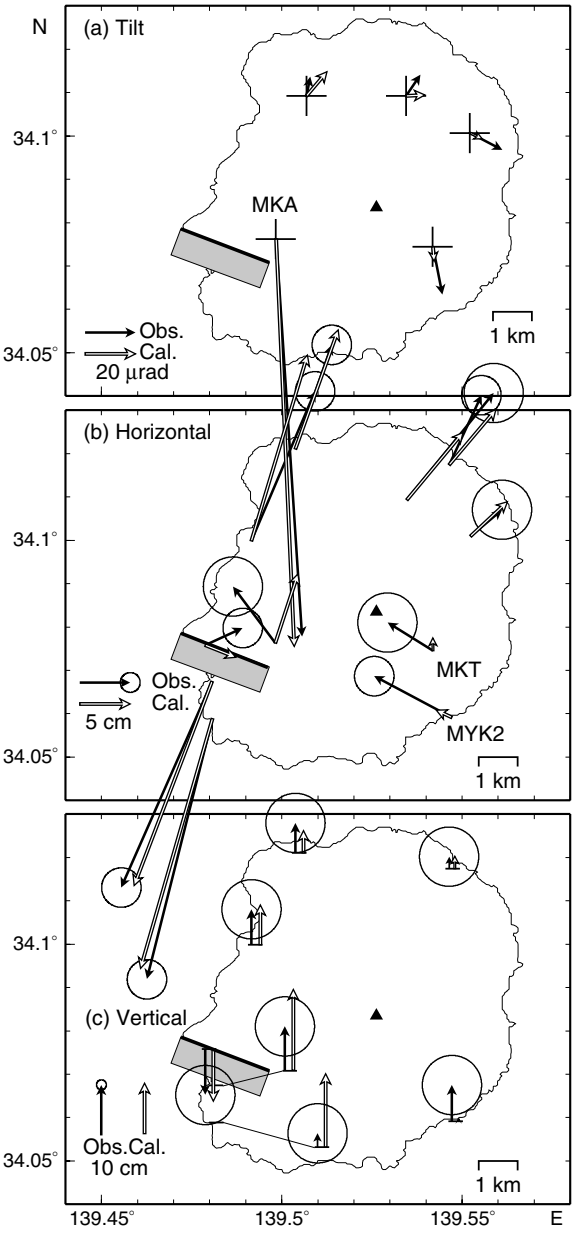

Figure 6. Observed crustal deformation of period 2 (21:00 LT on June 26—01:00 LT on June 27): (a) tilt-down vectors, (b) horizontal displacement and (c) vertical displacement vectors. Circles are standard errors of displacements. Blank arrows are the theoretical deformations calculated from the best-fitting dyke model, whose projection on the ground surface and the upper bound are shown by rectangles and thick lines, respectively. The triangle represents the summit of Miyakejima.

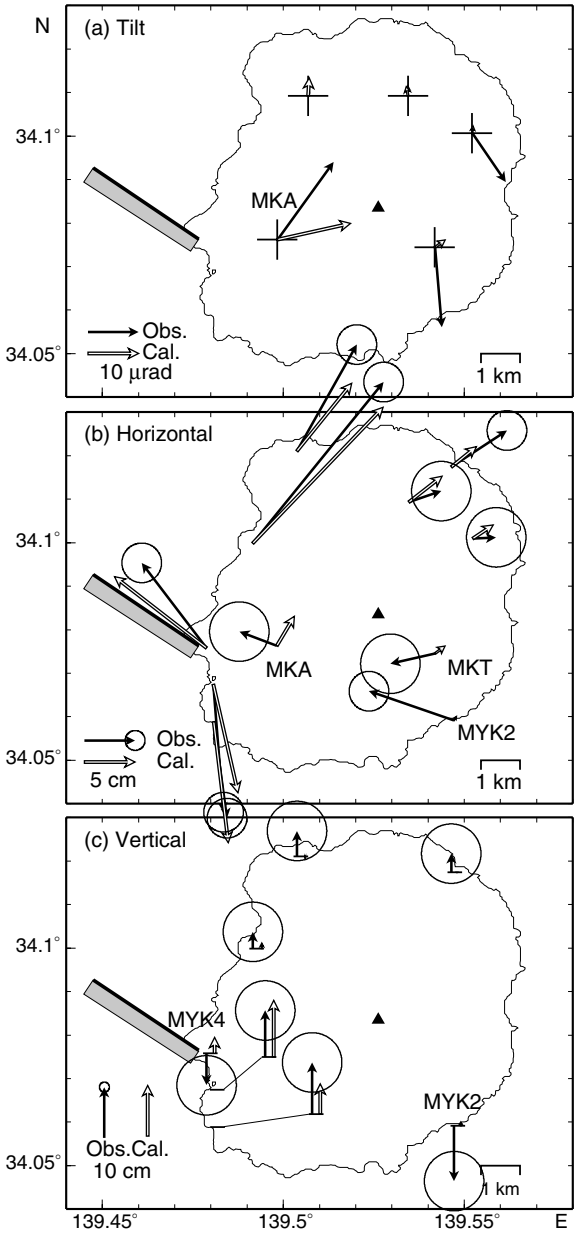

Figure 7. Observed crustal deformation of period 3 (01:00 LT—06:00 LT on June 27): (a) tilt-down vectors, (b) horizontal displacement and (c) vertical displacement vectors. Circles are standard errors of displacements. Blank arrows are the theoretical deformations calculated from the one-dyke model, whose projection on the ground surface and the upper bound are shown by rectangles and thick lines, respectively. The triangle represents the summit of Miyakejima.

was the principal cause, because the displacement vector patterns especially in periods 2 and 3 strongly suggest a dyke intrusion. Former studies by Fujita *et al.* (2002a) and Irwan *et al.* (2003) indicate that dyke opening can explain most of the crustal deformation. In this study, we estimate dyke configuration for the three time intervals, that is, periods 1, 2 and 3.

The previous studies suggest that dyke geometry changes in the course of the intrusion and propagation process with respect to the initial stage. Furthermore, the temporal change of the crustal deformation pattern indicates the contribution of a multidyke system to the volcanic activity. This variation in dyke geometry makes it difficult to estimate the dyke parameters because of too many unknowns. To obtain more reliable solutions, we adopted two steps in our estimation.

In the first step, one rectangular dyke is assumed to explain the deformation in each period. From the total change of the observation data in the period, we evaluated eight parameters defining a rectangular dyke: location of the centre of the top (latitude, longitude and depth), strike, dip, length, width and open dislocation (Fig. 8). As described in the next section, we add a contracting source with spherical or dyke geometry for periods 2 and 3, because a single-dyke model does not account satisfactorily for the observed data. The

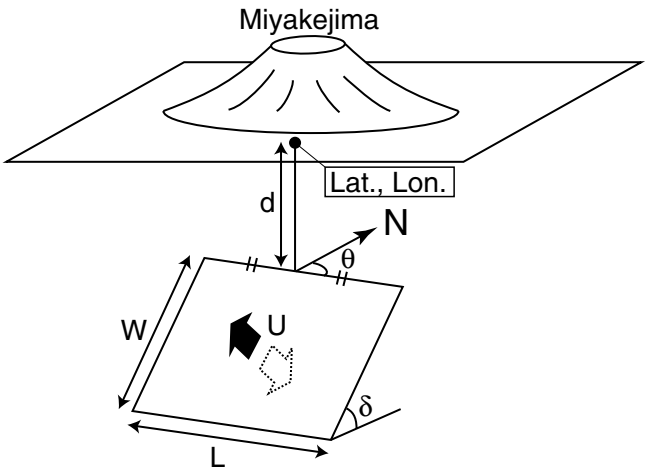

Figure 8. Definition of the eight unknown dyke parameters. d, θ, δ, L, W and U are the depth of the top, strike, dip angle, length, width and open dislocation, respectively.

estimated parameters are thought to express a dyke with a principal deformation in each period. We call these dykes principal dykes.

It is naturally considered that the deformation of the most dominant dyke was not limited to the time intervals we defined in Section 2. In the second step, using all of the time-series data, we estimate temporal change of the dislocation of the principal dykes over the whole duration of the initial stage in dealing with the other seven parameters of dykes (latitude, longitude, depth, strike, dip, length and width) as known.

In the first step, the eight parameters are estimated from the observed ground tilt changes and displacements by minimizing the fitness function:

$$f = \sum_{i=1}^{N} [O_i - C_i(\mathbf{m})]^2 / \sigma_i^2, \quad (1)$$

where N is number of data, O_i is ith data, C_i is ith synthetic deformation calculated from the dyke model parameter vector $\mathbf{m}$ and σ_i is the standard error of the ith data.

In eq. (1), the residuals between the observed and calculated deformation are normalized by their standard errors σ_i. The standard errors of the horizontal and vertical displacements of the dual-frequency GPS receivers are estimated to be 2 and 6 cm, respectively, while that of the horizontal displacement of the single-frequency receiver is 3 cm. We estimated the standard errors from the repeatability of station position during the period from 12:00 LT to 18:00 LT on June 26 before the crustal deformation started, following, for example, Williams *et al.* (1993). We adopted these values for eq. (1). The standard errors of the ground tilt observation are not clear. We performed the same analyses as we explain in this section for the three periods with the assumption of the standard error of 0.1, 0.5, 1 and 5 μrad. Assuming the standard error to be 1 μrad or less, we could obtain a source model that satisfied the tilt data but not the GPS data. In the present study, we adopted 5 μrad as the standard error. The value includes not only the uncertainty of the observation but also the discrepancy between the real Earth and modelling.

Because the function C_i in eq. (1) is non-linear with regard to dyke parameters other than opening, we adopted a genetic algorithm (GA; Appendix A) to find the best-fitting parameters. The C_i value in eq. (1) is calculated using an analytical expression formulated by Okada (1992), which assumes uniform opening of a rectangular dyke in a homogeneous isotropic elastic half-space. The search ranges of parameters are summarized in Tables 1, 2 and 3, corresponding respectively to periods 1, 2 and 3. The search range for the location of each dyke was set assuming that the earthquake swarm area was fully involved in the range.

3.2 Parameters of the principal dykes

The resulting parameters of the principal dykes are summarized in Tables 1, 2 and 3. Comparisons between the observed crustal deformation and the synthetic deformation calculated from the respective models are shown in Figs 5, 6 and 7. Projection of the dyke model on the ground surface and its upper bound are shown by rectangles and thick lines, respectively, in each figure.

The principal dyke model of period 1 is located on the southwestern flank of the island and dips to the southeast (Fig. 5). The dyke is directed towards the summit of Miyakejima. The calculated deformation fits the observations fairly well. Fig. 6 shows that the principal dyke of period 2 is very different from that of period 1. The dyke model is further west than that of period 1 and turns its strike clockwise by 70°. The depth of the top is very shallow, but it extends more deeply. This dyke model generally agrees with the characteristic deformation of period 2, the northeast–southwestward extension in the western and northern part of the island, and the large tilt change of MKA. However, the model does not explain the westward displacement at the southeastern part (MKT and MKY2). The principal dyke of period 3 has almost the same strike as that of period 2 and they join each other (Fig. 7). Although this model can explain the displacements in the western and northern parts of the island, except for the horizontal displacement of MKA and the

Table 1. The parameters of the dyke model of period 1 (DK1).

Parameters	Search ranges in GA		Best-fitting parameters	Confidence intervals of 68 per cent (95 per cent)	
	Lower	Upper		Lower	Upper
Latitude (°N)	34.05	34.09	34.074	34.067 (34.059)	34.079 (34.083)
Longitude (°E)	139.50	139.54	139.508	139.505 (139.500)	139.517 (139.526)
Depth (km)	0.0	5	1.7	0.4 (0.1)	1.72 (2.1)
Strike (°)	0.0	180	40.2	36.7 (22.6)	52.2 (64.9)
Dip (°)	0.0	180	62.8	38.1 (21.2)	63.4 (70.6)
Length (km)	0.0	10	2.4	0.7 (0.2)	4.5 (6.6)
Width (km)	0.0	10	0.9	0.5 (0.2)	3.6 (19.0)
Open (m)	0.0	5	1.8	0.6 (0.3)	4.1 (4.9)
Volumetric change (10^6 m^3)	—	—	3.9	2.4 (1.2)	6.4 (31.2)

Table 2. The parameters of the dyke model of period 2 (DK2).

Parameters	Search ranges in GA		Best-fitting parameters	Confidence intervals of 68 per cent (95 per cent)	
	Lower	Upper		Lower	Upper
Latitude (°N)	34.05	34.09	34.075	34.072 (34.070)	34.076 (34.078)
Longitude (°E)	139.46	139.52	139.484	139.482 (139.467)	139.491 (139.499)
Depth (km)	0.0	5	0.5	0.3 (0.1)	0.7 (1.3)
Strike (°)	0.0	180	110.7	102.4 (95.0)	112.5 (118.8)
Dip (°)	0.0	180	86.8	78.1 (72.7)	88.9 (93.8)
Length (km)	0.0	10	2.4	1.6 (0.8)	7.1 (9.4)
Width (km)	0.0	10	12.2	8.1 (2.5)	15.8 (29.0)
Open (m)	0.0	5	1.3	0.7 (0.5)	2.1 (4.1)
Volumetric change (10^6 m^3)	—	—	38.1	28.3 (16.5)	65.7 (132.1)

Table 3. The parameters of the one-dyke model of period 3.

Parameters	Search Ranges in GA		Best-fitting parameters
	Lower	Upper	
Latitude (°N)	34.05	34.09	34.085
Longitude (°E)	139.46	139.52	139.462
Depth (km)	0.0	5	0.3
Strike (°)	0.0	180	123.5
Dip (°)	0.0	180	65.8
Length (km)	0.0	10	3.2
Width (km)	0.0	10	0.9
Open (m)	0.0	5	3.6
Volumetric change (10^6 m^3)	—	—	10.6

subsidence of MYK4, it cannot explain the tilt changes, the westward displacements in the southeastern part (MKT and MYK2) and the subsidence at MYK2.

Because the one-dyke models of periods 2 and 3 do not agree with the crustal deformation in the southeastern part, we explore other models. The principal dykes do not contribute significantly to the crustal deformation in the southeastern part, suggesting the crustal deformation at MKT and MYK2 are probably originated from a different, additional source. Hence, we reconstruct dyke models with an additional source for periods 2 and 3.

We will try to compare the one-dyke model with two models consisting of two sources: one is a model with an intrusive dyke and a contracting dyke (DD case), and the other is that with an intrusive dyke and a contracting spherical source (Mogi 1958; DS case). The reasons we assume a contracting source is that we assume that a magma chamber supplied magma to the dykes. In addition to that, the westward displacement at the southeastern stations and the subsidence of MYK2 in period 3 suggest that a contracting source was present in the southern part.

We searched for best-fitting parameters for the models using a genetic optimization method similar to the one we used above. This method differs from that for the one-dyke model in two respects: first, a model of the DD case is coded by a string of 128 binary values; and secondly, the probability of mutation p_m is set at 0.025 (the definitions of binary value and p_m are given in Appendix A). A model of the DS case is coded by a string of 96 binary values, because the spherical source has four unknown parameters, the location of centre (latitude, longitude and depth) and volumetric change.

Because of clear differences of results on period 3, we explain the result on period 3 ahead of that on period 2. Tables 4 and 5 list the best-fitting parameters of the DD case and the DS case of period 3, respectively, summarizing the search ranges of parameters where we assumed that the contracting source was located in the southern part of the island. Comparisons between the observed and calculated deformation from the model are shown in Figs 9 and 10, respectively. The best-fitting model of the DD case explains fairly well the westward displacements at MKT and MYK2, the subsidence of MYK2, and the tilt changes as well as the displacement in the western and northern part (Fig. 9). The inflating dyke of the model is located to the west of the island and is similar to the one-dyke model. The best-fitting model of the DS case, by contrast, does not fit the westward displacement at MKT, the subsidence at MYK2 and the tilt changes (Fig. 10). It should be noted that the observed horizontal displacement and tilt vectors at MKT are perpendicular to each other. The perpendicular vectors are explained by the contracting dyke located at the southwestern side of the island (Fig. 9). In contrast, the perpendicular vectors cannot be explained by the contracting spherical source, because a spherical source causes horizontal displacements and tilt changes in the same radial direction (Fig. 10).

The Akaike's information criterion (AIC) parameters (Akaike 1974) of the DD case of period 3 are 223.9, which is far smaller than the best-fitting one-dyke model (AIC = 256.3) and the DS case (AIC = 234.9). We therefore adopt the two-dyke model (DD case) as the most appropriate principal dyke model for period 3.

The AIC parameters of the one-dyke model, the DD case and the DS case of period 2 are 235.8, 237.1 and 238.0, respectively. The complicated models do not improve the AIC of the one-dyke model for period 2. We adopt the one-dyke model as the most appropriate principal dyke model for period 2. However, the contracting dyke in period 3 probably began to contract in period 2 because the westward displacement of MKT and MYK2 and the southward tilt change of MKT began in period 2.

We hereafter refer to the principal dyke models of periods 1, 2 and 3, and the additional contracting dyke of period 3 as DK1, DK2, DK3 and DK4, respectively. The horizontal locations of DK1 to DK4 are summarized in Fig. 11(a).

3.3 The confidence interval of the dyke parameters

Because the parameters were obtained by means of a GA, confidence intervals of the parameters cannot be estimated in the conventional manner using a formula. In this study, therefore, we apply the bootstrap method (Efron & Tibshirani 1993) to assess the confidence intervals. The bootstrap method assumes that each data item is randomly sampled from an identical probability distribution. Because

Table 4. The parameters of the two-dyke model of period 3.

Parameters	Search ranges in GA		Best-fitting parameters	Confidence intervals of 68 per cent (95 per cent)	
	Lower	Upper		Lower	Upper
Inflating dyke (DK3)					
Latitude (°N)	34.05	34.09	34.088	34.079 (34.073)	34.089 (34.092)
Longitude (°E)	139.46	139.52	139.462	139.4615 (139.460)	139.473 (139.482)
Depth (km)	0.0	5	0.1	0.02 (0.0)	0.4 (1.1)
Strike (°)	0.0	180	131.2	106.9 (89.1)	131.3 (134.6)
Dip (°)	0.0	180	55.9	52.1 (48.9)	90.9 (105.3)
Length (km)	0.0	10	4.5	1.2 (0.6)	4.6 (5.0)
Width (km)	0.0	10	3.2	1.8 (0.7)	11.9 (18.7)
Open (m)	0.0	5	1.6	1.2 (0.6)	4.2 (4.9)
Volumetric change (10^6 m^3)	—	—	23.0	11.6 (6.2)	46.3 (74.3)
Contracting dyke (DK4)					
Latitude (°N)	34.06	34.09	34.0623	34.061 (34.056)	34.075 (34.087)
Longitude (°E)	139.48	139.54	139.503	139.491 (139.481)	139.522 (139.535)
Depth (km)	0.0	10	3.4	1.9 (0.4)	4.9 (6.9)
Strike (°)	0.0	180	15.5	11.8 (3.5)	62.3 (173.4)
Dip (°)	0.0	180	74.2	50.0 (24.0)	86.4 (137.8)
Length (km)	0.0	5	3.0	1.1 (0.4)	4.3 (5.3)
Width (km)	0.0	5	2.1	1.1 (0.4)	4.4 (6.9)
Open (m)	−5	0.0	−2.3	−4.4 (−4.9)	−1.2 (−0.4)
Volumetric change (10^6 m^3)	—	—	−14.5	−27.9 (−51.9)	−5.3 (−1.4)

Table 5. The parameters of the one-dyke and one spherical source model of period 3.

Parameters	Search Ranges in GA		Best-fitting parameters
	Lower	Upper	
Inflating dyke			
Latitude (°N)	34.05	34.09	34.086
Longitude (°E)	139.46	139.52	139.463
Depth (km)	0.0	5	0.05
Strike (°)	0.0	180	129.5
Dip (°)	0.0	180	57.6
Length (km)	0.0	10	4.2
Width (km)	0.0	10	5.0
Open (m)	0.0	5	1.5
Volumetric change (10^6 m^3)	—	—	31.5
Contracting spherical source			
Latitude (°N)	34.060	34.090	34.061
Longitude (°E)	139.500	139.530	139.532
Depth (km)	0.0	10	0.2
Volumetric change (10^6 m^3)	−100	0.0	−0.9

the present crustal deformation data involve different uncertainties, we resampled the weighted residuals between the observed and calculated deformation instead of the data items, based on the method of Cervelli *et al.* (2001). The procedure that evaluates the dyke parameters from the resampled residuals is the same as we used above, except that we do not simply minimize eq. (1), but eq. (1) replaced by resampled weighted residuals. We iterated the bootstrap calculations 2000 times, and obtained 68 and 95 per cent confidence intervals of the parameter by discarding the top and bottom 320 and 50 of the sorted parameters, respectively.

The confidence intervals of the dyke parameters of DK1 and DK2 are listed in Tables 1 and 2, respectively. The result for DK1 shows that the location of the centre of the top is limited to a shallow area 2 × 2 km on the southwestern flank of the island. This dyke is clearly directed towards the summit and dips to the southeast. The length, width and opening, unlike the other parameters, are not well constrained, as a result of the poor coverage of the stations in the southern part of the dyke. Although the 95 per cent confidence intervals of width and volumetric change are wide, their 68 per cent confidence intervals are 0.5–3.6 km and 2.4–6.4 × 10^6 m^3, respectively. DK2 is restricted to within a narrow area, which indicates DK2 to be an almost vertical dyke clearly striking to the ESE. The difference between DK1 and DK2 is clear. Although the 95 per cent confidence interval of width is rather wide, the parameter concentrates around 10 km and the 68 per cent confidence interval is 8.1–15.8 km. The length and opening are not well constrained because of the poor coverage of the stations in the western part of the dyke and because of the trade-off between them.

Table 4 shows the confidence intervals of DK3 and DK4. Although DK3 and DK4 are not well constrained, we believe DK3 is situated to the northwest of DK2 and that DK4 exhibits a configuration closer to that of DK1 than to DK2. The result shows that DK4 is directed to the north or northeast and is located in the southwestern part of Miyakejima. For a few parameters, the estimated 95 per cent confidence intervals are equivalent to the search ranges of GA (e.g. the longitude of DK3). This is because the GA occasionally selects a value near the boundary of the search range with respect to a weakly constrained parameter and then the Levenberg–Marquardt method is conducted with the value as an initial value. Because the search ranges of parameters affect the confidence intervals for the weakly constrained parameters, we possibly underestimated the confidence intervals with respect to these parameters.

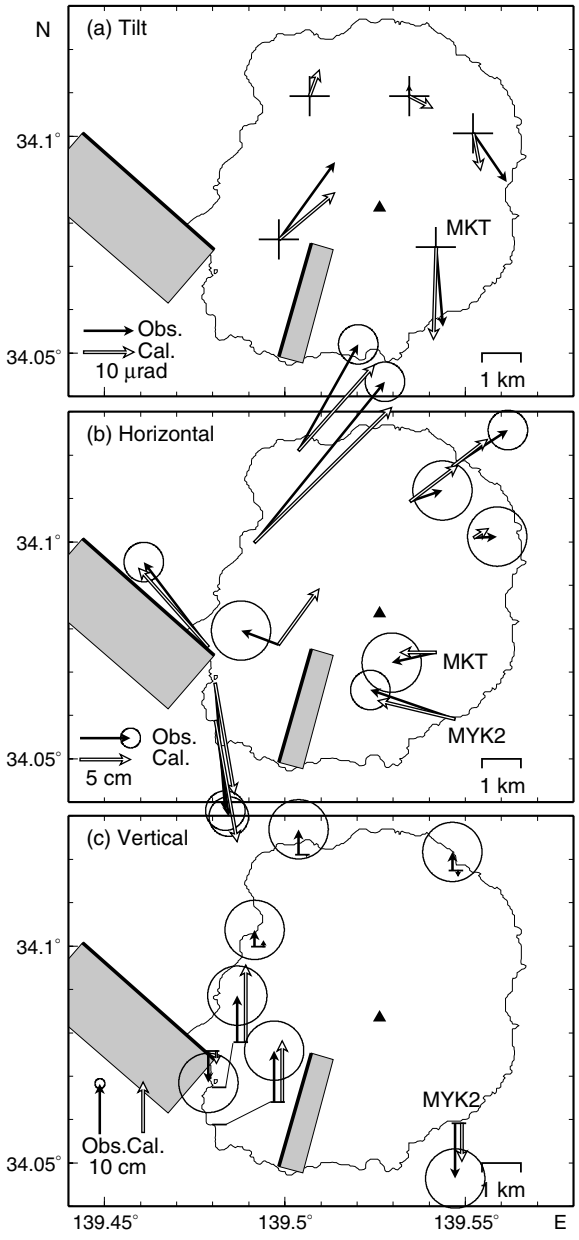

Figure 9. Comparison between the two-dyke model of period 3 (01:00 LT—06:00 LT on June 27) and the observed crustal deformation: (a) tilt-down vectors, (b) horizontal displacement and (c) vertical displacement vectors. Circles are standard errors of displacements. Blank arrows are the theoretical deformation calculated from the model, whose projection on the ground surface and the upper bound are shown by rectangles and thick lines, respectively. The triangle represents the summit of Miyakejima.

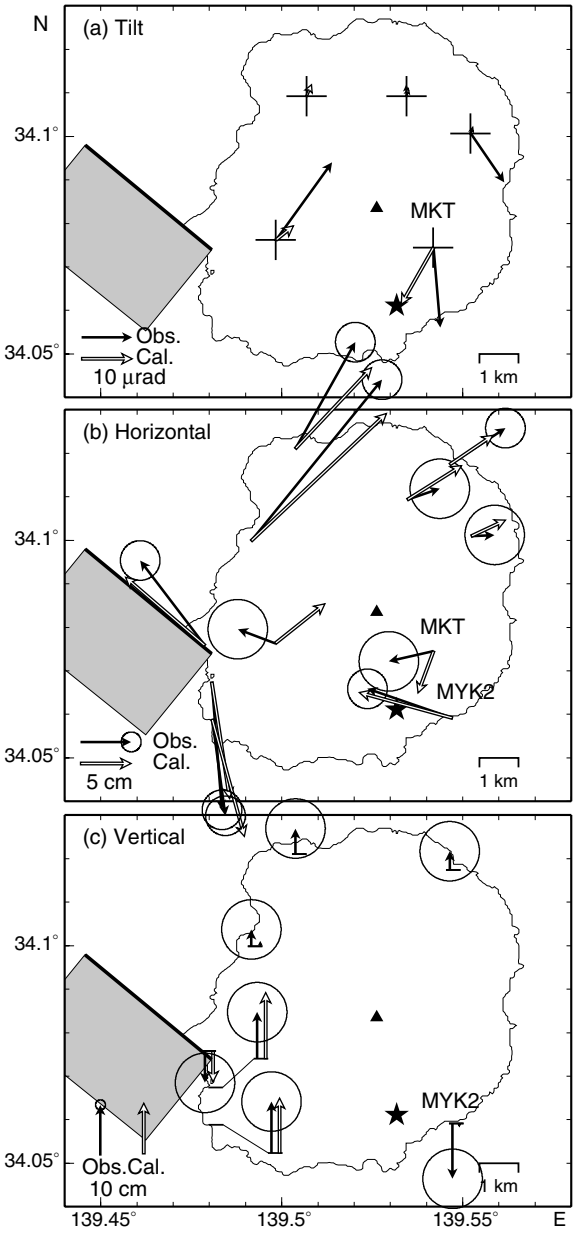

Figure 10. Comparison between the one-dyke with one spherical source model of period 3 (01:00 LT—06:00 LT on June 27) and the observed crustal deformation: (a) tilt-down vectors, (b) horizontal displacement and (c) vertical displacement vectors. Circles are standard errors of displacements. Blank arrows are the theoretical deformation calculated from the model. The projection of dykes on the ground surface and location of the spherical source are shown by rectangles and stars, respectively. The triangle represents the summit of Miyakejima.

3.4 Adjustment of the dyke model to the time-series data

The dyke configurations estimated in the previous section are probably too simplified, because the total changes in the observed data in each period are modelled assuming one or two principal dykes. This is a rather oversimplified assumption, because the dyke opening and contraction would not cease within each period. In this section, we attempt to estimate the active periods of the principal dykes by adjusting the model to the time-series data. Because the principal dykes are likely to be connected to a common magma chamber and conduit, accurate active periods are needed to find the relationship between the principal dykes.

To adjust the model, we approximate a change of opening of each dyke using a quadratic step function as follows:

$$u(t) = \begin{cases} \frac{2U}{T^2}(t - t_0)^2 & \text{for} \quad t_0 \le t < \frac{t_0+t_1}{2} \\ U - \frac{2U}{T^2}(t - t_1)^2 & \text{for} \quad \frac{t_0+t_1}{2} \le t < t_1, \end{cases} \tag{2}$$

where: $u(t)$ is opening of each dyke at time t; t_0 and t_1 are the starting and termination time of dyke opening, respectively; U is the cumulative opening at t_1; and T is the duration time of the opening ($T = t_1 - t_0$). The function is a simple increasing or decreasing function as shown in the inset in the upper left side of Fig. 11(b). We

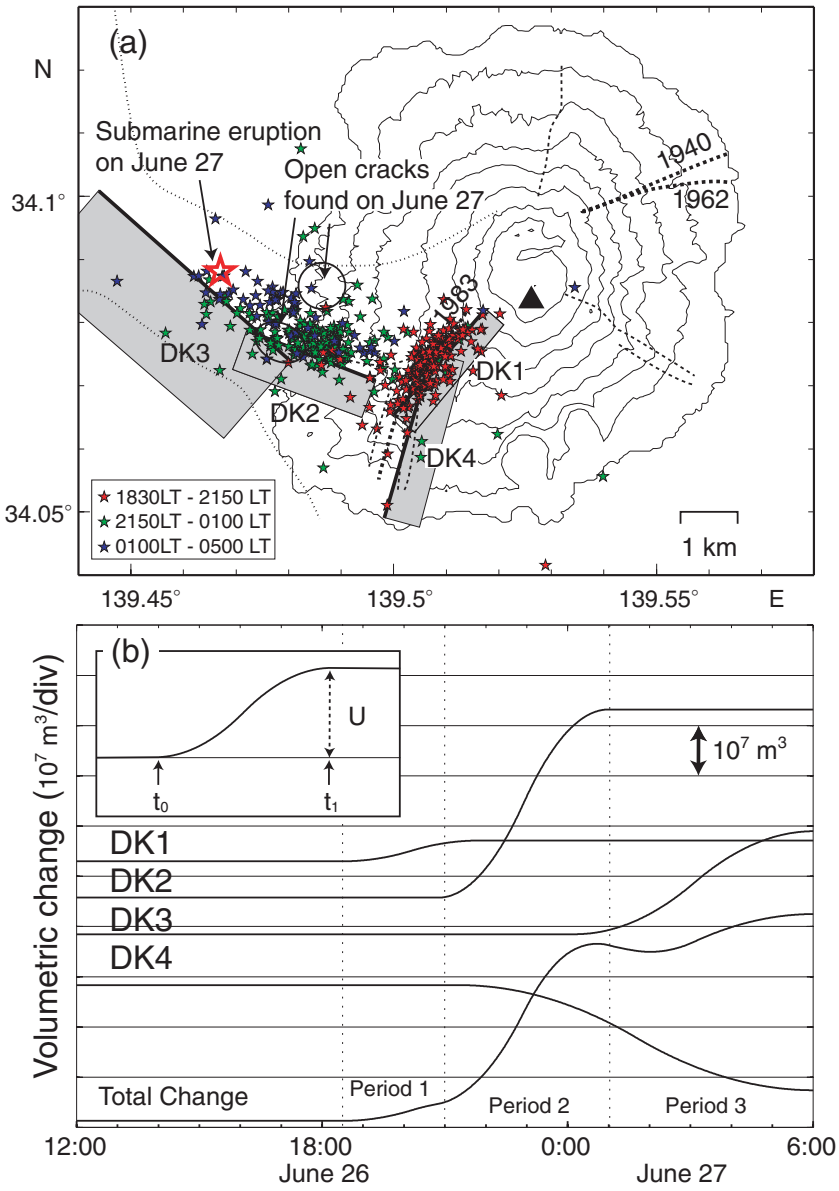

Figure 11. (a) Projections of the principal dykes on the ground surface (rectangles). Small stars show the earthquake distribution during 18:30 LT on June 26 to 05:00 LT on June 27 (Uhira *et al.* 2005). Dotted curves show an area where DK2 and DK3 cause tensional stress change in NE–SW direction on the ground surface. Broken lines represent fissures formed after the 15th century (after Tsukui *et al.* 2001). The triangle denotes the summit of Miyakejima. (b) Time-series of volumetric changes of the four principal dykes. Vertical lines are bounds of the periods. Inset: an assumed quadratic time function on the opening of each dyke. t_0 and t_1 are the beginning and termination time of opening, and U is the opening at t_1.

assume that parameters other than opening did not change. Although this assumption may seem slightly strong, because the dykes might have changed not only their thicknesses but also their length and width during the propagation, we can still approximate the period of the dyke intrusion and time-series of volumetric change of each dyke.

The appropriate t_0 and t_1 of each dyke are simultaneously estimated by a grid search method with 10-min intervals so as to minimize eq. (1), in which O_i and C_i are observed and the deformation calculated every minute. Because the function C_i in eq. (1) is linear with regard to U, if t_0 and t_1 are given, U can be uniquely determined by the linear least-squares method. In the estimation, we assumed that t_0 of DK1 is 18:30 LT on June 26, and t_1 of DK3 and DK4 is 06:00 LT on June 27, respectively.

The estimated t_0, t_1 and U of each dyke are listed in Table 6. The time-series of calculated deformation from the obtained time function of the dyke opening are shown in Figs 2 and 3 for the tilt change and the kinematic GPS data, respectively. Despite the simplicity of the model, we are able to fit the overall pattern of the crustal deformation reasonably well. The model is a good approximation of the source of the crustal deformation. Some details of the features do not fit particularly well. For example, the calculated tilt changes generally agree with the observed data, but their residuals exceeded approximately 10 μrad at the northern stations. The synthetic displacement generally agrees with the observations other than some stations with residuals of 3 and 5 cm for the horizontal and vertical displacements, respectively. The calculated horizontal displacement at MKA diverges from the observed displacement. These

Table 6. The active periods of the dykes.

Dykes	Active periods t_0	Active periods t_1	Open (m)
DK1	**18:30** LT	21:50	1.8
DK2	20:50	01:00	1.3
DK3	00:10	**06:00**	1.4
DK4	21:20	**06:00**	−3.3

Bold parameters are fixed in the curve fitting.

discrepancies are probably the result of differences between the reality and our simplified model: rectangular dykes with uniform openings in a homogeneous isotropic elastic half-space and their opening obey a simple time function, whereas the sizes and locations are fixed.

Fig. 11(b) shows the volumetric changes in the dykes, calculated from the estimated time-series of the opening. The intrusion of DK1 began at 18:30 LT on June 26 and stopped at around 21:00 LT. DK2 began to intrude at around 21:00 LT. It is noticeable that the contraction of DK4 also began at around 21:00 LT, because the westward displacement at the southeastern stations and the southward tilt change of MKT had already started in period 2. At around 01:00 LT on June 27, the intrusion of DK2 stopped and DK3 began to intrude. Because DK3 is located at the northwestern extension of DK2 and they join each other, the intrusion of DK3 probably exhibits continuous lateral propagation of DK2 towards the northwest. Although the width of DK3 is shorter than that of DK2, they can be close because the width of DK3 is poorly constrained.

3.5 Comparison with the seismicity

The crustal deformation at the initial stage began and coincided with the occurrence of the earthquake swarm. The earthquakes may have been induced by dyke intrusions into the shallow brittle crust. As the mechanisms of the dyke-induced earthquake swarms, pore pressure increases in the crust by pressure increase of fluid in the dykes and stress change in the crust as a result of the intrusion have been proposed (e.g. Ukawa & Tsukahara 1996), which suggest that the distribution of earthquakes correlates with the location and direction of the dyke. We can confirm the validity of our dyke model by comparing it with the seismicity.

Fig. 11(a) shows a comparison of between our dyke model and the epicentres accurately determined by Uhira *et al.* (2005) with the Double-Difference method (Waldhauser & Ellsworth 2000). The epicentres in the period from 18:30 LT to 21:50 LT are distributed along a line running 2 km southwest from the summit. The location and azimuth of the distribution during the DK1 intrusion are very similar to those of DK1. The swarm ceased at around 21:50 LT and moved to the west coast. At the same time, the intrusion of DK1 terminated and DK2 began to intrude. The epicentres at the west coast are distributed along a band in the WNW–ESE direction. The location and direction coincide with DK2 and DK3 within the estimation error for the dykes. The dyke model and the earthquake swarm have a strong spatial and temporal correlation. The notable aspect of the earthquake swarm is that the westward movement of the swarm area at 21:50 LT was not continuous but an abrupt movement. There was an obscure gap of earthquakes between the two active swarm areas. This aspect coincides with the fact that DK1 and DK2 are separate dykes. This strong correlation indicates that the configurations of dykes can be closely estimated using crustal deformation data.

4 DISCUSSION

4.1 Magma migration process in the initial stage

On the basis of the location and temporal volumetric changes of the four dykes, DK1 to DK4, we can reconstruct the magma migration process in the initial stage as follows.

(i) In period 1, the first dyke intrusion, DK1, took place at the southwestern flank of Miyakejima. The dyke is directed to the summit and its top depth is less than 2 km (Table 1).

(ii) In period 2, the dyke intrusion at the southwestern flank ceased and instead a new dyke intrusion began beneath the west coast of the island, DK2. This dyke is almost vertical and its top depth reaches 0.5 km from the ground surface. This dyke is characterized by its high width down to a depth of approximately 10 km (Table 2). As in the following period, DK3 began at the western end of DK2, so the magma migration direction in period 2 can be concluded to be from east to west.

(iii) In period 3, dyke extension to the northwest direction from the western end of DK2 is suggested by DK3. The top of the dyke is very shallow, probably shallower than 1 km (Table 4), while the width was not well constrained. Because of the similarity in configuration between DK2 and DK3, we believe the magma migration direction of DK3 to be northwestward.

Our questions regarding the magma migration process are now focused on the source supplying the magma to dykes DK1 to DK3. First, we consider the case of DK1. Because the locations of DK1 and DK4 are close to each other, and DK4 is deeper than DK1, the most probable source for DK1 is DK4. DK4 is probably a dyke-shaped magma chamber, because it contracted at the initial stage.

However, the temporal volumetric change of DK4 indicates the contraction of DK4 began just before the halt of the intrusion of DK1 as shown in Fig. 11(b), not supporting the magma supplying from DK4 to DK1. We consider the following three possible causes.

(i) Magma was supplied from DK4. The contraction of DK4 with comparable volumetric change to DK1 could not be detected because of the assumption of the time function of eq. (2) and resolution of the present estimation.

(ii) Magma was supplied from DK4. The contraction of DK4 was small as a result of a vesiculation of magma.

(iii) Magma was supplied from a deeper magma source than DK4.

To investigate the possibility of DK4 as a source for DK1, we evaluate a two-dyke model consisting of DK1 and DK4 for period 1 with a condition that the inflation volume of DK1 is equal to the contraction volume of DK4. The parameters of DK4 other than the opening are the same as those estimated in Section 3. The resulting parameters of DK1 including volumetric change, which is estimated to be 5.4×10^6 m^3 in this case, are within the 95 per cent confidence intervals estimated in Section 3. The AIC parameter of the present two-dyke case (189.0) is almost the same as that of one-dyke case (189.7) in Section 3, meaning that the information from the observation is not enough to judge whether DK4 contracted in period 1 or not. In fact, the tilt change and horizontal displacement at MKT caused by the contraction of DK4 with the above volume change

are 6 μrad and 1.5 cm, approximately 16–20 per cent of the observed deformation. Although, this analysis cannot distinguish the three possibilities (i), (ii) and (iii), we infer that DK4 is the source of DK1, considering that DK1 is located above DK4.

The dyke-shaped magma chamber DK4 has been suggested by previous studies. Crustal deformation observed before the activity of 2000 suggests the existence of a dyke-shaped inflating source striking to the summit in the southwestern part of Miyakejima. Kimata (2001) suggests from the horizontal displacement in Miyakejima during the period 1998–1999 that there was an inflating dyke at the depth range of 3–5 km beneath the southwestern part of the island. Murakami *et al.* (2001) also suggested this from the levelling data in the period 1997–1999. A gravity change associated with the activity of 2000 also suggests a contracting dyke that is directed towards the summit at the southwestern part (Okubo *et al.* 2000). Although the location of DK4 is not well constrained, DK4 is probably identical to the inflating and contracting dyke. However, a further investigation of crustal deformation and thermal studies of magma is needed to elucidate how long the dyke had existed.

Secondly, we consider the magma budget among DK2, DK3 and DK4 to identify a source supplying the magma to DK2 and DK3. Fig. 11(b) indicates that the total inflated volume of DK2 and DK3 are approximately 3 times larger than that of the contraction of DK4, suggesting possibilities of another magma source or inflation as a result of vesiculation during the course of migration. Saito *et al.* (2005) showed that the magma drastically vesiculated in the depths shallower than 3 km from the melt inclusion analysis of the ejecta at the largest eruption of 2000 August 18. The bottom depth of DK2 reaches around 10 km (Table 2), and that of DK3 is possibly close to it because of the similarity between DK2 and DK3. These results indicate that most of the magmas in DK2 and DK3 moved below 3 km, that is, the effect of vesiculation is not significant in the dyke intrusions of DK2 and DK3. Hence, we conclude that the large deficit of magma supply from DK4 to DK2 and DK3 comes from magmas supplied by another magma chamber located deeper than DK4.

The former studies based on GPS data estimated the magma chamber of Miyakejima to being at the depth of 4.2 km (Nishimura *et al.* 2001) or 12 km (Ito & Yoshioka 2002). Based on the GPS data and the tilt data after the initial stage, we recently revealed that the magma chamber consists of two parts: a shallow dyke-shaped chamber (DK4) ∼4–6 km deep and a deep spherical chamber ∼7–10 km deep beneath DK4 (Ueda *et al.* 2005). The deep chamber probably corresponds to the main source supplying magmas to DK2 and DK3. The petrological study by Saito *et al.* (2005) also suggests the presence of a deep magma chamber at the depth of 10 km.

The dyke model suggests that a magma of $\sim 3 \times 10^7$ m^3 was supplied from the deeper chamber. This is possibly the largest estimate because we do not take account of inflation of magma as a result of vesiculation. The spherical source with a contraction of 3×10^7 m^3 causes crustal deformation at the observation stations no more than 7.5 μrad (tilt), 3 cm (horizontal displacement) and 7.5 cm (vertical displacement). The amount of deformation is close to the standard errors of each data set. Therefore, it is difficult to detect the deflation of the deeper chamber at the initial stage.

Fig. 12 schematically shows the magma migration process inferred from our result. DK1 began to intrude from the dyke-shaped magma chamber (DK4) towards the southwestern flank of Miyakejima at 18:30 LT on June 26. At around 21:00 LT, the westward migration of magma (DK2) started. Considering the gap of dykes between DK2 and DK4 (Fig. 11a), and the seismicity gap between DK2 and DK4 (Fig. 11a), we infer that a large amount of magma was supplied directly from the deep chamber to DK2 and DK3 as shown in Fig. 12. The magma in DK4 drained into the deep chamber, causing the contraction of DK4. The intrusion of DK1 ceased at around 21:00 LT on June 26, simultaneously with the beginning of the intrusion beneath the west coast. This synchronization was

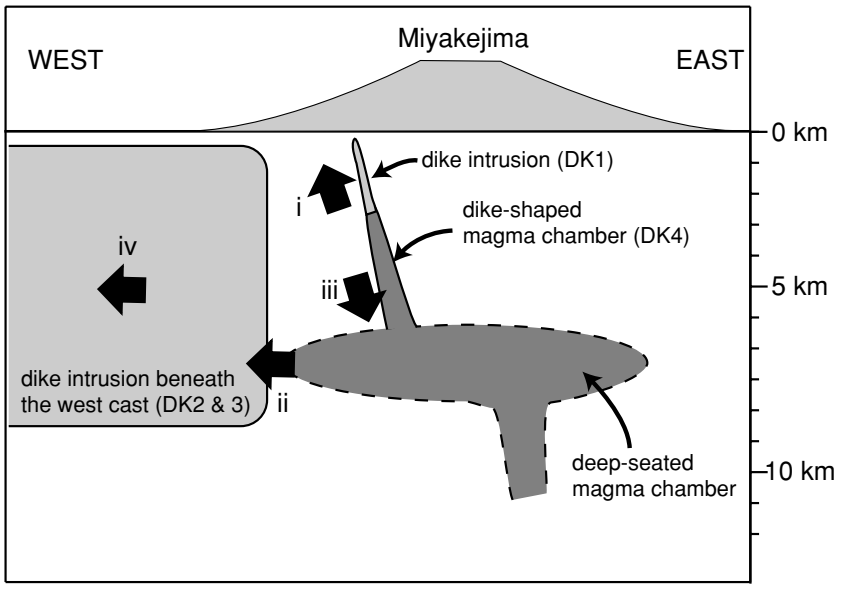

Figure 12. Schematic illustration of the magma migration process at the initial stage inferred from the dyke model. (i) At 18:30 LT on June 26, magma began to intrude towards the southwestern flank of Miyakejima from the dyke-shaped magma chamber. (ii) At around 21:00 LT, a large volume of magma began to intrude from the deep-seated chamber to beneath the west coast. (iii) Accompanied by the discharge of magma from the deep chamber, the magma in the shallow chamber drained into the deep chamber. The deflation of the shallow chamber terminated the initial intrusion at around 21:00 LT. (iv) The dyke beneath the west coast gradually propagated towards the northwest.

probably originated from the reduced pressure in DK4 as a result of the magma outflow towards the northwest.

After the initial stage, the propagation of the dyke towards the northwest continued, with its length reaching 30 km (Sakai *et al.* 2001). The magma that moved from beneath Miyakejima to the southwest had amounted to ∼0.7 km^3 until late August (Nishimura *et al.* 2001). The magma probably flowed through DK2 and DK3, and the discharge of magma from the chamber resulted in the collapse-caldera formation after the initial stage (Geshi *et al.* 2002).

Our magma migration process model suggests that if the intrusion of DK2 had not occurred, the intrusion of DK1 might not have terminated. The intrusion might have continued and resulted in a fissure eruption on the flank of Miyakejima. The fissure eruption was typical among the other eruption until the last eruption of 1983, but did not occur in the 2000 activity. The outflow of magma from the magma chamber resulted in the collapse-caldera formation after the initial stage (Geshi *et al.* 2002). The caldera formation was for the first time in 2500 yr (Tsukui *et al.* 2001). The style of the 2000 eruptive activity has been primarily changed compared with the past eruptions by the discharge of magma towards the northwest.

4.2 Surface phenomena and dyke intrusions

At the initial stage, several visible phenomena associated with the magma movement were found on the ground surface. Comparing these observations with our magma migration model, we discuss the causes of those phenomena.

At 08:30 LT on July 27, discoloured water was noticed 1.2 km off the west coast of Miyakejima (see Fig. 11a for its location), where submarine craters were later found on the ocean floor (Shirao *et al.* 2000). The ejected magma amounted to 5000 m^3. The discoloured water was found near DK3 after the intrusion of DK3; the depth of the top of DK3 is very shallow. Therefore, the submarine eruption was probably a small eruption of magma in the upper tip of DK3.

On the west coast of Miyakejima, open cracks and graben structures with strikes of N50°W–N60°W were found on June 27 (see Fig. 11a for their locations; Kawanabe *et al.* 2002). The cracks are located near DK2 and DK3, and the strikes of cracks coincide with those of the dykes. The area between the dotted curves in Fig. 11(a) is an area where DK2 and DK3 cause tensional stress change in the NE–SW direction on the ground surface, including the fracture areas. The stress change is strong especially just above the dyke. The crack openings might have been led by the strong tensional stress change. The strong stress change is also shown by a large magnetic field change recoded at MKA, which is explained by the piezomagnetic effect associated with the dyke intrusion (Ueda *et al.* 2003).

4.3 Comparison between the dykes and the stress field around Miyakejima

The direction of a dyke intrusion is sensitive to local stress fields in the vicinity of the dyke (Nakamura 1984). Because the directions of DK1 and DK2 are quite different, we need to compare the directions of dykes with the stress fields to justify the dyke model and discuss the cause of the dyke intrusion.

Dykes tend to intrude perpendicularly to the minimum principal stress axis and expand in parallel to the maximum principal stress axis. In Miyakejima, the eruptive flank fissures that had formed in past eruptions are distributed radially from the summit and the fissures gradually curve to the NW–SE with increasing distance from the summit (see Fig. 11a). The distribution was interpreted by Nakamura (1984) as the result of the stress field in Miyakejima. The radial distribution is a result of the local stress field caused by expansion of magma chamber beneath Miyakejima. The curve to the NW–SE is the result of the regional stress field in the southern Izu islands, where strike-slip earthquakes with NW–SE compression axes and NE–SW tension axes are predominant. The regional stress field is interpreted as originating in the bending of the Philippine Sea Plate at the northern Izu peninsula (Nakamura 1984) or a collision of the Philippine Sea Plate with the Eurasian Plate (Ukawa 1991). DK1 and DK4, which are relatively close to the summit, are directed to the summit, and DK2 and DK3 are directed to the NW–SE direction and are normal to the NE–SW tension axes in the southern Izu islands. The directions of the four dykes are a logical result of the local stress field in Miyakejima.

The horizontal intrusion of magma is often seen in rift zones, such as in Krafla Volcano, Iceland (e.g. Einarsson & Brandsd-ttir 1980) and Kilauea Volcano, Hawaii (e.g. Wallace & Delaney 1995; Rubin *et al.* 1998). In the case of Krafla Volcano, Einarsson & Brandsd-ttir (1980) suggest that the primary driving force is the tectonic stress that has built up on the plate boundary in Iceland. In Miyakejima, because DK2 and DK3 intruded perpendicular to a minimum principal stress axis and parallel with a maximum principal stress axis of the regional stress field, the lateral intrusion might be similar to these cases. Buoyancy is not likely to be a driving force behind the lateral intrusion. Lateral propagation continued after the initial stage, and a dyke 30 km long and 2–8 m thick intruded off the west coast of Miyakejima until 2000 September (Nishimura *et al.* 2001). If we assume that this dyke intrusion, which is large enough to change the eruptive style of Miyakejima, was the result of accumulated intraplate stress, a long time would have been needed to build up this level of stress, possibly far longer than the eruption intervals of 20 yr; this is consistent with the fact that the type of the 2000 eruptive activity is markedly different from that of recent eruptions in the 20th century (Tsukui *et al.* 2001). The lateral intrusion in Miyakejima might be caused by not only the excess pressure of the magma chamber but the regional stress field, which had accumulated over an extended period as a result of the movement of the Philippine Sea Plate.

5 CONCLUSIONS

We have constructed a source model that approximately explains the continuous tilt and GPS observations at the initial stage of the 2000 Miyakejima activity (18:30 LT on June 26—06:00 LT on June 27). The source model consists of four dykes, of which three are intruding dykes and one is a contracting dyke. Based on the dyke model, we inferred the magma migration process at the initial stage as follows. At 18:30 LT on June 26, the magma began to ascend from a dyke-shaped magma chamber and intrude at the southwestern flank of Miyakejima. In this intrusion, the total volume of magma was $\sim 4 \times 10^6$ m^3. At around 21:00 LT, a relatively large volume of magma began to intrude beneath the west coast. The dyke propagated laterally towards the northwest. The intruded magma amounted to $\sim 40 \times 10^6$ m^3 up to 01:00 LT. This large intrusion caused discharge of magma from the magma chamber and this discharge terminated the first intrusion at the southwestern flank. The northwestward propagation of the dyke and the contraction of the chamber continued thereafter.

The activity of 2000 is radically different from the style characteristic of other recent eruptions, which have been fissure eruptions on the flank of the volcano. The style of eruptive activity of 2000

has been changed primarily by the large intrusion beneath the west coast. This large intrusion appears to have terminated the first intrusion that had been ascending towards the flank of Miyakejima. The discharge of a large volume of magma from the magma chamber resulted in the formation of a collapse caldera after the initial stage.

ACKNOWLEDGMENTS

We are grateful to K. Uhira for providing us with the hypocentral data. We thank Professor T. Dahm and anonymous reviewers for their thorough reviews and helpful comments. We also thank Y. Okada for his continuous encouragement and M. Kikuchi for helping us to use the tilt data.

REFERENCES

Akaike, H., 1974. A New Look at the Statistical Identification Model, *IEEE T. Automat. Contr.,* **19,** 716–723.

Cervelli, P., Murray, M.H., Segall, P., Aoki, Y. & Kato, T., 2001. Estimating source parameters from deformation data, with an application to the March 1997 earthquake swarm off the Izu Peninsula, Japan, *J. geophys. Res.,* **106,** 11 217–11 237.

Efron, B. & Tibshirani, R.J., 1993. *An introduction to the bootstrap, Monographs on statistics and applied probability 57,* Chapman & Hall/CRC, Boca Raton, p. 436.

Einarsson, P. & Brandsd-ttir, B., 1980. Seismological evidence for lateral magma intrusion during the July 1978 deflation of the Krafla Volcano in NE-Iceland, *J. Geophys.,* **47,** 160–165.

Fujita, E., Ukawa, M., Yamamoto, E. & Okada, Y., 2002a. Scenarios of dike intrusions at the beginning of the Miyakejima volcano activities, *Bull. Earthq. Res. Inst.,* **77,** 67–75.

Fujita, E., Ukawa, M., Yamamoto, E. & Okada, Y., 2002b. Cyclic jerky opening of magma sheet and caldera formation during the 2000 Miyakejima volcano eruption, *Geophys. Res. Lett.,* **29,** 10.1029/2001GL013848.

Geshi, N., Shimano, T., Chiba, T. & Nakada, S., 2002. Caldera collapse during the 2000 eruption of Miyakejima Volcano, Japan, *B. Volcanol.,* **64,** 55–68.

Irwan, M., Kimata, F., Fujii, N., Nakao, S., Watanabe, H., Ukawa, M., Fujita, E. & Kawai, K., 2003. Rapid crustal deformation caused by magma migration in the Miyakejima Volcano, Japan, *Earth Planets Space,* **54,** e13–e16.

Ito, T. & Yoshioka, S., 2002. A dike intrusion model in and around Miyakejima, Niijima and Kozushima in 2000, *Tectonophysics,* **359,** 171–187.

Kariya, S. *et al.*, 2000. Crustal movement on Miyakejima detected by GPS measurement—Joint GPS data analysis observed by ERI, GSI, NIED, JMA and JHD—, *Prog. Abst. 2000 fall meet. Seism. Soc. Jpn.,* A15 (in Japanese).

Kawanabe, Y., Matsushima, K., Hayashi, S., Kaneko, T. & Nakada, S., 2002. Open cracks found at Miyakejima on June 27, 2002, *Rep. Coord. Comm. Pred. Volc. Erupt.,* **78,** 64–65 (in Japanese).

Kimata, F., 2001. Magma intrusion system estimated from the ground deformation at Miyake Volcano in and after the 1983 eruption, *Abst. 2001 Japan Earth Planet. Sci. Joint Meeting,* V0–004.

Kumagai, H., Ohminato, T., Nakano, M., Ooi, M., Kubo, A., Inoue, H. & Oikawa, J., 2001. Very-long-period seismic signals and caldera formation at Miyake Island, Japan, *Science,* **293,** 687–690.

Mitchell, M., 1996. An introduction to genetic algorithms, The MIT Press, Cambridge, MA, p. 209.

Miyazaki, T., 1984. Features of historical eruption at Miyake-jima Volcano, *Bull. Volcano. Soc. Jpn.,* **29,** S1–S15 (in Japanese with English abstract).

Mogi, K., 1958. Relations between the eruptions of various volcanoes and the deformations of the ground surface around them, *Bull. Earthq. Res. Inst.,* **36,** 99–134.

Murakami, M., Nishimura, T. & Ozawa, S., 2001. Crustal deformation associated with the 2000 eruption of Miyake volcano and earthquake swarm near Kozu island, *Geographical Survey Institute Journal,* **95,** 115–120 (in Japanese).

Nakada, S. *et al.*, 2001. Chronology of the Miyakejima 2000 eruption: Characteristics of summit collapsed crater and eruption products, *J. Geogr.,* **110,** 168–180.

Nakamura, K., 1984. Distribution of flank craters of Miyake-jima Volcano and the nature of the ambient crustal stress field, *Bull. Volcano. Soc. Jpn.,* **29,** S16–S23 (in Japanese with English abstract).

Nishimura, T., Ozawa, S., Murakami, M., Sagiya, T., Tada, T., Kaidzu, M. & Ukawa, M., 2001. Crustal deformation caused by magma migration in the northern Izu Islands, Japan, *Geophys. Res. Lett.,* **28,** 3745–3748.

Okada, Y., 1992. Internal deformation due to shear and tensile faults in a half-space, *Bull. seism. Soc. Am.,* **82,** 1018–1040.

Okubo, S., Furuya, M., Sun, W., Tanaka, Y., Watanabe, H., Oikawa, J., Maekawa, T. & Oshima, H., 2000. Spatio-temporal gravity variation during the 2000 volcanic activity of the Miyakejima Volcano, Japan (2), *Prog. Abst. 2000 fall meet. Seism. Soc. Jpn.,* A18 (in Japanese).

Rubin, A.M., Gillard, D. & Got, J., 1998. A reinterpretation of seismicity associated with the January 1983 dike intrusion at Kilauea Volcano, Hawaii, *J. geophys. Res.,* **103,** 10 003–10 015.

Saito, G., Uto, K., Kazahaya, K., Shinohara, H., Kawanabe, Y. & Satoh, H., 2005. Petrological characteristics and volatile content of magma from the 2000 eruption of Miyakejima Volcano, Japan, *B. Volcanol.*, **67,** 268–280.

Sakai, S. *et al.*, 2001. Magma migration from the point of view of seismic activity in the volcanism of Miyake-jima Island in 2000, *J. Geogr.,* **110,** 145–155.

Sato, H., Takahashi, H., Yamamoto, E., Fukuo, N., Uehara, M. & Terasawa, Y., 1980. Development of the crustal tilt observation method using borehole-type tiltmeters, *Zisin,* **33,** 343–368.

Seno, T., Stein, S. & Gripp, A.E., 1993. A model for the motion of the Philippine Sea Plate consistent with NUVEL-1 and geological data, *J. geophys. Res.,* **98,** 17 941–17 948.

Shirao, M. *et al.*, 2000. Submarine observation of undersea craters in Miyakejima 2000 eruption, *Prog. Abst. Volcano. Soc. Jpn.,* A5.

Tsukui, M., Niihori, K., Kawanabe, Y. & Suzuki, Y., 2001. Stratigraphy and formation of Miyakejima Volcano, *J. Geogr.,* **110,** 156–167.

Ueda, H., Matsumoto, T., Fujita, E., Ukawa, M., Yamamoto, E., Sasai, Y., Irwan, M. & Kimata, F., 2003. Geomagnetic change associated with the magma intrusion at the initial stage of the 2000 activity of Miyakejima, Central Japan, *EOS, Trans. Am. geophys. Un.,* **84**(46), Fall Meet. Suppl., Abstract, V51J–0411.

Ueda, H., Fujita, E., Ukawa, M., Nishimura, T. & Murakami, M., 2004. Estimation of a source model of crustal deformation related with the 2000 Miyakejima eruptive activity, *Abst. 2004 Japan Earth Planet. Sci. Joint Meeting,* V055–P022.

Uhira, K., Baba, T., Mori, H., Katayama, H. & Hamada, N., 2005. Earthquake swarms preceding the 2000 eruption of Miyakejima Volcano, Japan, *B. Volcanol.*, **67,** 219–230.

Ukawa, M., 1991. Collision and fan-shaped compressional stress pattern in the Izu block at the northern edge of the Philippine Sea plate, *J. geophys. Res.,* **96,** 713–728.

Ukawa, M. & Tsukahara, H., 1996. Earthquake swarms and dike intrusion off the east coast of Izu Peninsula, central Japan, *Tectonophysics,* **253,** 285–303.

Ukawa, M., Fujita, E., Yamamoto, E., Okada, Y. & Kikuchi, M., 2000. The 2000 Miyakejima eruption: Crustal deformation and earthquakes observed by the NIED Miyakejima observation network, *Earth Planets Space,* **52,** xix–xxvi.

Waldhauser, F. & Ellsworth, W.L., 2000. A double-difference earthquake location algorithm: Method and application to the northern Hayward fault, *Bull. seism. Soc. Am.,* **90,** 1353–1368.

Wallace, M.H. & Delaney, P.T., 1995. Deformation of Kilauea volcano during 1982 and 1983: A transition period, *J. geophys. Res.,* **100,** 8201–8219.

Williams, C.R., Arnadottir, T. & Segall, P., 1993. Coseismic deformation and dislocation models of the 1989 Loma Prieta earthquake derived from global positioning system measurements, *J. geophys. Res.,* **98,** 4567–4578.

APPENDIX A: A GENETIC ALGORITHM TO SEARCH THE BEST-FITTING DYKE PARAMETERS

We employed a GA (Mitchell 1996) to search for dyke parameters, because it is a useful technique for this type of study. Because the function C_i in eq. (1) is non-linear with regard to the dyke parameters other than opening, we solved a non-linear least-squares problem to obtain the best-fitting parameters. This form of problem is often solved by the use of methods based on derivatives of an objective function with respect to the parameters such as the steepest decent method, the Gauss–Newton method and the Levenberg–Marquardt method. If appropriate starting parameters are given, the method can quickly and accurately find a best-fitting parameter. Because the objective function of this study has numerous local minima, derivative-based methods risk converging on a local minimum rather than the global minimum. Moreover, the solution is strongly influenced by the starting model. Other methods that thoroughly search the whole parameter space cost a lot of time to find the best-fitting parameters. Because Monte Carlo algorithms, including GA, are not based on derivatives, they carry a relatively low risk of converging on the wrong local minimum. Although GA randomly tests various model parameters over a wide search area, it progressively modifies the search area in the parameter space, and efficiently and rapidly finds high-potential areas within the parameter space. One advantage of a Monte Carlo algorithm is that it generally starts from randomly generated parameters. The starting model does not depend on *a priori* information, so we can compare the final model with other geological and geophysical observations.

In GA, the model parameters are coded as genes and a large population of models composed of genes is searched to achieve a best-fitting model. A group of models is generated first and then the GA modifies the group as if they were evolving in a biological system. The degree to which the model fits the observed data is quantitatively evaluated with an objective function. The best pair of models is selected on the basis of the function and then a pair of offspring is generated from the parents according to probabilistic rules. This process is iterated over numerous generations until the fit becomes sufficiently high. Consequently, the fitness of the group is improved efficiently and rapidly.

In this study, we coded a model using one chromosome, formed from eight genes that correspond to the eight model parameters. We then divided the search range of the parameter by 256 and assigned binary values to each. A gene is coded with eight figures of binary values and corresponds to a point in the search range of the parameter. For example, because we searched for the best-fitting dip angle of a dyke in the range from 0° to 180°, 00000000 and 11111111 correspond to 0° and 180°, respectively. Fig. A1(a) schematically shows a dyke model expressed as a string of 64 binary values. The binary values are converted to real values when the objective function is evaluated. The reason a gene is coded with eight binary values

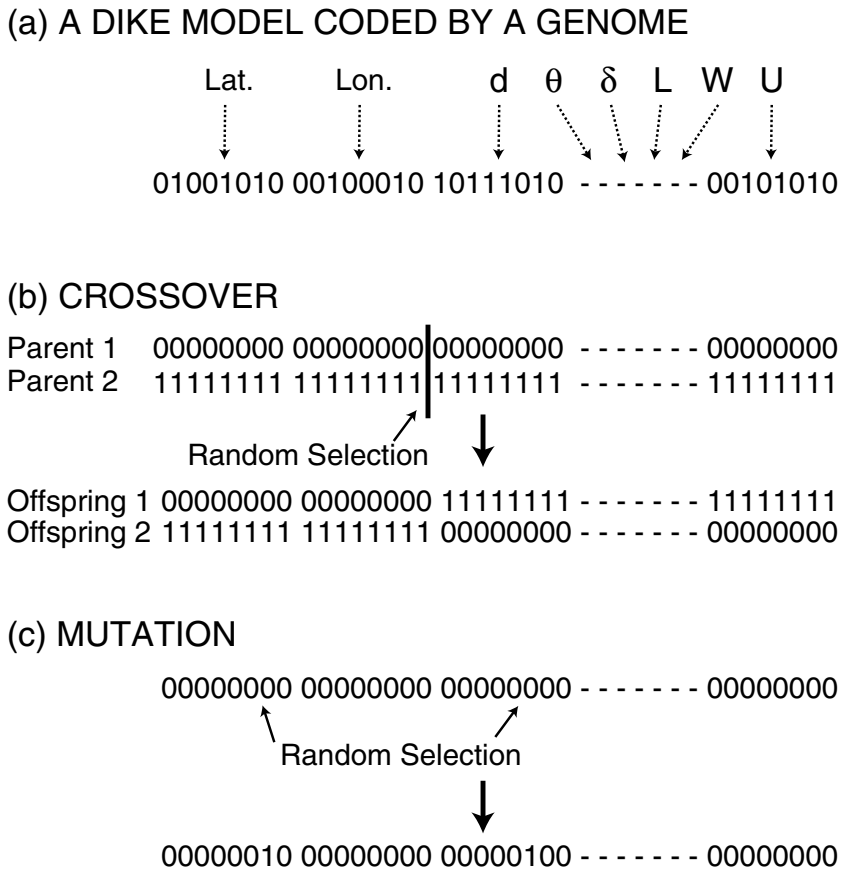

Figure A1. Schematic views of (a) a dyke model coded by binary values in a genetic algorithm (GA) and the operations of a GA: (b) crossover and (c) mutation.

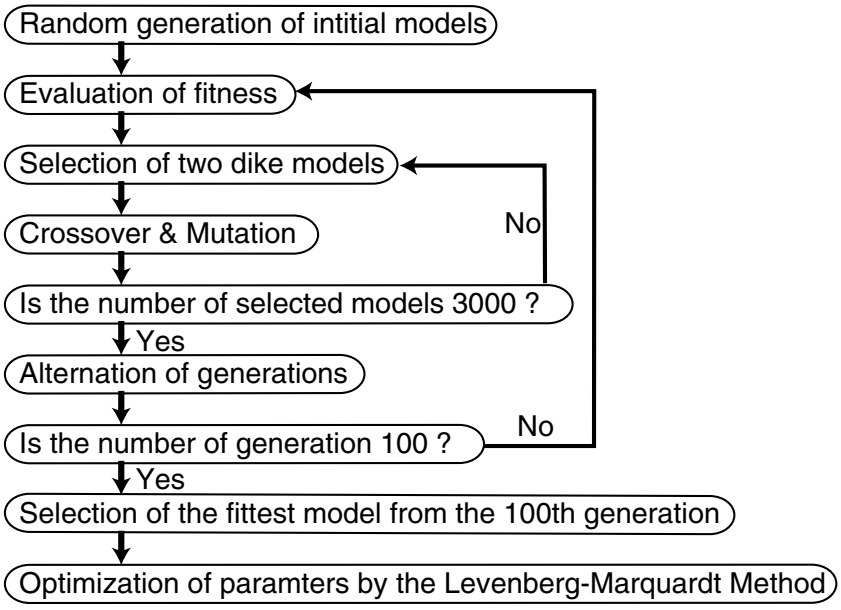

Figure A2. Flowchart of the optimization program of dyke parameters with the genetic algorithm (GA).

is that a search range can be finely divided and it is easy to handle programming-wise.

Fig. A2 schematically shows a flowchart of our program. First, we randomly generate 3000 initial models. These models are measured for their fitness to the observed data by the fitness function eq. (1). Based on their fitness, we select a pair of relatively good models with a probability of selection $p_s = f_i^{-1} / \sum_{j=1}^{3000} f_j^{-1}$, where f_i is the fitness function of the ith model ($i = 1, 2, \ldots 3000$). This pair produces two offspring by crossover and mutation. Crossover is the exchange of genes of the models, as schematically shown in Fig. A1(b). Divisions of genes are first randomly selected in a pair of chromosomes, and then a new chromosome is combined with the left-hand portion of one old chromosome and the right-hand portion of the other old chromosome. The combination of the remains of the old chromosomes make another new chromosome. The probability of occurrence of crossover is p_c. If it does not occur, the parents are copied to the offspring in their entirety. Mutation alters the offspring randomly as shown schematically in Fig. Al(c). The mutation independently changes each of the bits in the models with a probability of p_m. The selection, crossover and mutation process is iterated until the total number of the offspring reaches 3000. The new generation of models is measured by the fitness function for what degree they fit the observed data. The process is repeated for 100 generations and the fittest model in the 100th generation is selected. In this study, we further apply the Levenberg–Marquardt method using the fittest model as the starting model to find the best-fitting model without fixing the search range of the parameter. Using the hybrid method with the derivative-based algorithm, we can correct errors as a result of the dividing and limitation of the search range, and accurately find the exact local minimum. Because GA does not always converge on the global minimum, we execute this calculation several times to find the global minimum.

We empirically use 0.5 and 0.05 as p_c and p_m, respectively. If the probabilities are too high, good genes do not easily descend to the offspring and the calculation does not converge rapidly enough. If the probabilities are too small, the models do not easily improve and the calculation does not home in on the best-fitting model fast. We carried out several tests with different probabilities and selected the most efficient value for convergence. We added a specific procedure to improve the performance of the GA. The worst model of a generation is exchanged with the fittest model of the preceding generation. This operation prevents the loss of good genes by crossover and mutation, and thus promotes rapid convergence.